



# Improved supercapacitor application of manganese ferrite nanoparticles via co-precipitation technique

Abisha D<sup>a,c</sup>, Gibin S.R<sup>a,c,\*</sup>, PremKumar V.K<sup>b</sup>, Mariappan A<sup>a,c</sup>

<sup>a</sup> Department of Physics and Research Centre, Malankara Catholic College, Mariagiri, Kaliakkavilai-629153, Tamil Nadu, India

<sup>b</sup> Laboratory of Electrochemical Energy Storage, Institute of Environmental Resources Engineering Zhejiang University, China

<sup>c</sup> Manonmaniam Sundaranar University, Abishekapatti-627012, Tirunelveli, Tamil Nadu, India

## ARTICLE INFO

### Keywords:

Manganese ferrite  
Co-precipitation  
Structural properties  
Super capacitor  
BET  
Cyclic voltammetry

## ABSTRACT

The novel co-precipitation technique has been employed to create the manganese ferrite nanoparticle. The prepared sample was annealed for various temperatures 400 °C, 600 °C and 700 °C. Based on TG/DT analysis the optimal temperature was found to be 700 °C and further additional analysis was performed for the sample annealed at 700 °C. Their morphology and properties were determined using SEM, HR-TEM, EDX, FTIR, XPS, BET, and CV techniques. Using the X-ray diffraction technique, the prepared sample's structural characteristics were demonstrated. The SEM as well as HR-TEM images showed the nanoparticles had a roughly spherical shape. The EDX analysis confirmed the presence of the elements Fe, O, and Mn in the sample; there was no evidence of contamination by other elements. The specific surface area of the nanoparticles was estimated by BET analysis, which provides details of the material's porosity and surface area. The binding energy of the sample was estimated using XPS measurements, which provide details on the composition and chemical states of the individual elements. By using cyclic voltammetry, the nanoparticles' electrochemical characteristics were evaluated. For a reduced scan rate of 2 mVs<sup>-1</sup>, the specific capacitance value was discovered to be 341 Fg<sup>-1</sup>, confirming their suitability for super capacitor applications.

## 1. Introduction

Nanotechnology is a relatively new field, research on the nanometre scale had a long existence. Since then, there has been a surge in exploring different technologies for making nanostructures and nanomaterials [1]. Research on magnetic nanoparticles has been conducted for basic biological purposes and future applications. Magnetic devices, switching devices, magnetic refrigeration, ferrofluid, catalysts, and other biomedical applications are just a few applications for the nanocrystalline spinel ferrite magnetic material. MnFe<sub>2</sub>O<sub>4</sub> is an important magnetic alloy which can be used as a catalyst, super capacitor, gas sensor, and inductance component [2]. Several techniques can be used to create the nanomaterials. The properties of nanomaterials can vary depending on their size and form due to their high surface-to-volume ratio and quantum confinement effects, and they can be employed for a range of applications [3].

The various methods used to generate MnFe<sub>2</sub>O<sub>4</sub> nanoparticles are co-precipitation, sol-gel, microemulsion, and mechanochemical processing which have been extensively studied [4]. The features of manganese ferrite are strongly reflected in its composition,

\* Corresponding author. Department of Physics and Research Centre, Malankara Catholic College, Mariagiri, Kaliakkavilai-629153, Tamil Nadu, India. Tel.: +91 9894469432.

E-mail address: [gibin.physics@gmail.com](mailto:gibin.physics@gmail.com) (G. S.R.).

<https://doi.org/10.1016/j.heliyon.2023.e21120>

Received 14 July 2023; Received in revised form 29 September 2023; Accepted 16 October 2023

Available online 20 October 2023

2405-8440/© 2023 Published by Elsevier Ltd. This is an open access article under the CC BY-NC-ND license (<http://creativecommons.org/licenses/by-nc-nd/4.0/>).

morphology, and size. The co-precipitation method is an attractive approach for producing nano ferrites due to its advantages in terms of improved purity and reactivity. This technique is relatively simple, cost-effective, and facilitates the production of uniformly sized and homogeneous nanoparticles with semi-spherical shapes. Furthermore, co-precipitation also provides compositional flexibility and can be easily scaled up for extensive study [5]. This method involves simultaneous nucleation, growth, coarsening, and agglomeration steps.

Nanostructured ferrite materials have unique properties apart from their bulk counterparts, because of fundamental changes in structure, electronic rearrangements, and the pronounced influence of surface atoms [6]. In addition to significantly improving the electrical and physiochemical qualities needed for storage devices like supercapacitors and batteries, nanotechnology is a term that is widely used to describe revolutionary developments in various fields of technology [7]. Supercapacitors are emerging as a highly promising energy storage solution, offering distinct advantages over conventional options like batteries and dielectric capacitors. Their exceptional attributes, including superior renewable energy integration, high power density, robust performance, and extended lifespan, position them as a compelling alternative [8,9].

Often referred to as ultracapacitors, supercapacitors utilize two distinct methods for storing electrical energy, each corresponding to their unique storage behavior. Electric double-layer capacitors (EDLCs), which use electrostatic attraction of opposing charges at the interface between the electrode and electrolyte to store energy, are the first approach. This leads to energy storage in an electrostatic fashion. The second method centers around electrochemical processes and relies on pseudocapacitive materials. These materials, such as conducting polymers, metal sulfides, and metal oxides, enable energy storage through electrochemical reactions [10,11]. Because it has an excellent electrochemical performance, a high theoretical capacitance, and is environmentally friendly, manganese is the most promising electrode material among other energy storage materials. It also has several oxidation states, including  $\text{Mn}^{2+}$ ,  $\text{Mn}^{3+}$ ,  $\text{Mn}^{4+}$ , and  $\text{Mn}^{6+}$  [12].

This study involved the synthesis and analysis of manganese ferrite nanoparticles using a novel co-precipitation method. Manganese nitrate, ferric nitrate, citric acid and sodium hydroxide were used as major components in this synthesis. Subsequently, the synthesized samples were annealed at temperatures of 400 °C, 600 °C, and 700 °C for 3 h. The samples were characterised using X-ray diffraction (XRD) analysis. Based on TG/DT analysis additionally, the sample annealed at 700 °C underwent further characterization using Scanning electron microscope (SEM), High-resolution transmission electron microscope (HR-TEM), Cyclic voltammetry (CV), Brunauer-Emmett-Teller (BET) analysis, Fourier transform infrared spectroscopy (FTIR), and X-ray photoelectron Spectroscopy (XPS). These characterization techniques provided valuable information on the structural, morphological, electrochemical, surface area, and chemical characteristics of the manganese ferrite nanoparticles.

## 2. Materials and methods

### 2.1. Synthesis of $\text{MnFe}_2\text{O}_4$ nanoparticles

The precursor for the formation of  $\text{MnFe}_2\text{O}_4$  nanoparticles was prepared through a novel co-precipitation process, using  $\text{MnFe}_2\text{O}_4$  as the precipitant. All chemicals were sourced from Merck Chemicals. Firstly,  $\text{Mn}(\text{NO}_3)_2 \cdot 4\text{H}_2\text{O}$ ,  $\text{Fe}(\text{NO}_3)_3 \cdot 9\text{H}_2\text{O}$ , and citric acid ( $\text{C}_6\text{H}_8\text{O}_7$ ) were separately dissolved in 20 ml of deionized water at different concentrations of 0.1 M, 0.2 M and 0.29 M respectively. Sodium hydroxide (NaOH) was slowly added drop by drop to the mixture, which was stirred at 3 h for 80 °C. The presence of citric acid behaved as a chelating agent during the process, resulting in the development of brown-coloured precipitates. The precipitates were widely cleaned multiple times using deionized water and acetone. Subsequently, they were dried at 80 °C to obtain dark brown precipitates. Finally, the precipitates were subjected to calcination at various temperatures for 3 h in a furnace.

### 2.2. Characterisation

The X-ray diffraction (XRD) analysis was examined to assess the crystalline phase of the  $\text{MnFe}_2\text{O}_4$  nanoparticles utilising an instrument BRUKER USA D8 Advance, Davinci with  $\text{CuK}\alpha$  radiation ( $\lambda = 1.54060 \text{ \AA}$ ), operating at 40 kV and 30 mA. The step scans were recorded for  $2\theta$  value in an angular range of 20°–80° at 10°/min scan speed. Phase identification was carried out using the International Centre for Diffraction Data (ICDD) database. The degradation behaviour of the synthesized sample was assessed using a thermal gravimetric and differential thermal analysis (TG/DTA) conducted with a NETZSCH-STA 449 F3 JUPITER instrument. Fourier transform infrared (FTIR) spectroscopy was performed using Purkin Elmer model Spectrum Two. The characterization purposes, a scanning electron microscope (SEM) have been performed with CAREL ZEISS EVO 18 model was utilized after sputtering the sample. Additionally, a High-resolution transmission electron microscope (HR-TEM) was coupled to Energy dispersive X-ray spectroscopy (EDX) was employed. The High-Resolution Transmission Electron Microscope (HR-TEM) was used with model FEI – TECNAI G<sup>2</sup>- 20 TWIN (operating voltages 200 kV) to investigate the morphology and determine the size. The elemental analysis was executed using Energy Dispersive X-ray Spectroscopy (EDX) using the instrument Bruker EDX with an  $\text{LN}_2$  free detector. The Selected Area Electron Diffraction (SAED) pattern was obtained by distributing the synthesized sample into a carbon-coated copper grid. The X-ray photoelectron spectroscopy (XPS) measurements were carried out using ULVAC - PH1 INC model PH150000 version probe 111. The Brunauer Emmett Teller (BET) was used to investigate the pore size and surface area employing Quantachrome Instruments, Autosorb IQ series. To assess the electrochemical properties, cyclic voltammetry (CV) was performed using a Versa STAT MC model.

### 3. Result and discussion

#### 3.1. Thermogravimetric and differential thermal analysis (TG/DTA)

The sample was subjected to simultaneous Thermogravimetric and differential thermal analysis (TG/DTA) in the temperature range between 35 °C and 800 °C. The TG/DTA curve indicating the behaviour of the prepared sample is illustrated in Fig. 1.

During the analysis, the first weight loss of about 8 % was observed between 70 °C and 325 °C. This weight loss can be attributed to the emission of water molecules from the sample. The second weight loss of around 10 % occurred between 325 °C and 500 °C, which was attributed to the decomposition of organic templates present in the sample. Furthermore, the third weight loss of roughly 2 % was observed in the temperature between 500 °C and 670 °C, which can be attributed to a phase transition within the sample. No notable weight loss was noticed beyond 670 °C, indicating the formation of manganese ferrite within the sample [13]. The DTA curve shows a minor endothermic peak around 125 °C, indicating the occurrence of dehydration. Additionally, an exothermic peak at 540 °C was observed which suggests the decomposition of nitrates present in the sample [14].

#### 3.2. X-ray diffraction (XRD)

The X-ray diffraction (XRD) patterns of manganese ferrite nanoparticles prepared using the co-precipitation method are illustrated in Fig. 2.

The XRD spectra display the annealed samples of  $\text{MnFe}_2\text{O}_4$  at various temperatures, namely 400 °C, 600 °C, and 700 °C. The XRD pattern analysis conclusively verified the occurrence of the  $\text{MnFe}_2\text{O}_4$  phase in the synthesized nanoparticles. The diffraction peaks detected in the XRD pattern were successfully matched and indexed to the common reference pattern [ICDD Card No (00-010-0319)] [15,16]. The specific  $2\theta$  values corresponding to the diffraction peaks were determined as follows 21.61°, 30.06°, 32.196°, 37.873°, 44.87°, 52.81°, 57.320°, 64.54°, 67.74° and 77.41° shows the crystal planes (111), (220), (311), (222), (400), (422), (511), (440), (620) and (622), respectively.

The presence of narrow and highly intense peaks in the XRD pattern confirms the high crystallinity and reduced dimensions of the prepared nanoparticles. Debye-Scherrer's equation was used to determine the average crystalline size [17].

$$D = \frac{K\lambda}{(\beta \cos\theta)} \quad (1)$$

Here, D stands for the crystalline size in nanometers, K denotes the diffraction constant ( $k = 0.9$ ),  $\lambda$  denotes the wavelength of the incident X-ray,  $\beta$  is calculated based on the full width at half maximum of the diffraction peak, and  $\theta$  signifies the diffraction angle. By using Debye-Scherrer's equation, the calculated average crystalline size of the  $\text{MnFe}_2\text{O}_4$  nanoparticles was found to be approximately 37 nm [18].

#### 3.3. Fourier transform infrared spectroscopy (FTIR)

The FTIR spectra of  $\text{MnFe}_2\text{O}_4$  covering a range of 4000 - 400  $\text{cm}^{-1}$  are exposed in Fig. 3. The FTIR analysis provides valuable insights into the functional groups existing in the substance and their related stretching frequencies. A prominent peak around 1600  $\text{cm}^{-1}$  is attributed to the bending vibration of the H–O–H bond in water molecules [19]. The peak observed at 443.08  $\text{cm}^{-1}$  reveals the stretching vibration of metal oxide bonds at the octahedral site, while the peak around 558.35  $\text{cm}^{-1}$  is associated with the stretching vibration of metal oxide bonds at the tetrahedral sites. Additionally, the peak at 1654.54  $\text{cm}^{-1}$  signifies the asymmetric stretching vibration of the O–C–O bond [20]. A high frequency absorption peak was found at 1718  $\text{cm}^{-1}$ , confirming the presence of O–H groups

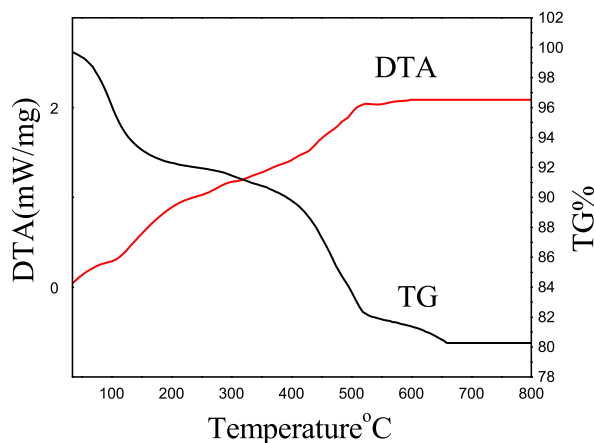


Fig. 1. TG/DT analysis curve of manganese ferrite nanoparticles.

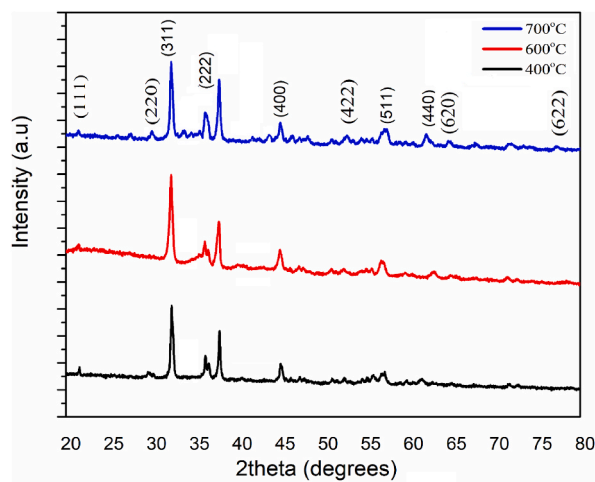


Fig. 2. XRD pattern for  $\text{MnFe}_2\text{O}_4$ .

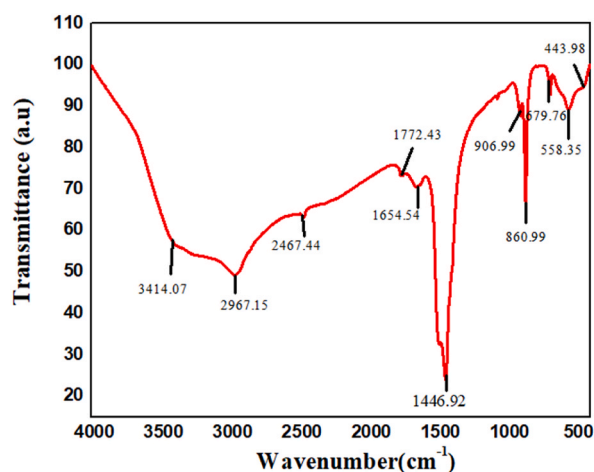


Fig. 3. FTIR spectra of  $\text{MnFe}_2\text{O}_4$ .

in the sample [24]. The spectra also exhibit absorption bands below  $1000\text{ cm}^{-1}$ , which are characteristic features of ferrite materials. Moreover, a band near  $1446.92\text{ cm}^{-1}$  indicates the C–H bending modes. The peak at  $3414.07\text{ cm}^{-1}$  reveals the O–H stretching vibration of the absorbed water molecule [21].

#### 3.4. Scanning electron microscope (SEM)

Fig. 4 (a, b and c) indicates the SEM images of  $\text{MnFe}_2\text{O}_4$  nanoparticles after annealing at  $700\text{ }^\circ\text{C}$ , providing insights into the surface morphology [22]. The images disclose that the grains exhibit a roughly spherical-like shape, indicating a unique microstructure. Notably, a significant number of atoms are observed within the grains, indicating a high atom density [23].

#### 3.5. High-resolution transmission electron microscope (HR-TEM)

Fig. 5 (a) and (b) show the HR-TEM images of the sample annealed at  $700\text{ }^\circ\text{C}$ , enabling a closer examination of the particle size and surface morphology. The images were used at different magnifications to offer detailed insights. The HR-TEM image of  $\text{MnFe}_2\text{O}_4$  nanoparticles had a roughly spherical shape, accompanied by slight agglomeration within the sample [24]. SAED pattern reveals a ring-like structure made up of bright points, indicating the highly polycrystalline nature and excellent crystallinity of the manganese ferrite nanoparticles. The SAED pattern is exposed in Fig. 5 (c). The average particle size was examined by comparing the crystallite size acquired via XRD using the Debye-Scherrer equation. Using image 'j' viewer software an average particle size was determined to be around  $35\text{ nm}$  [25]. This size estimation is visually illustrated in Fig. 5 (d) and graphically presented in the bar diagram shown in Fig. 5 (e). Table 1 displayed the determined average particle size made using the image 'j' viewer software.

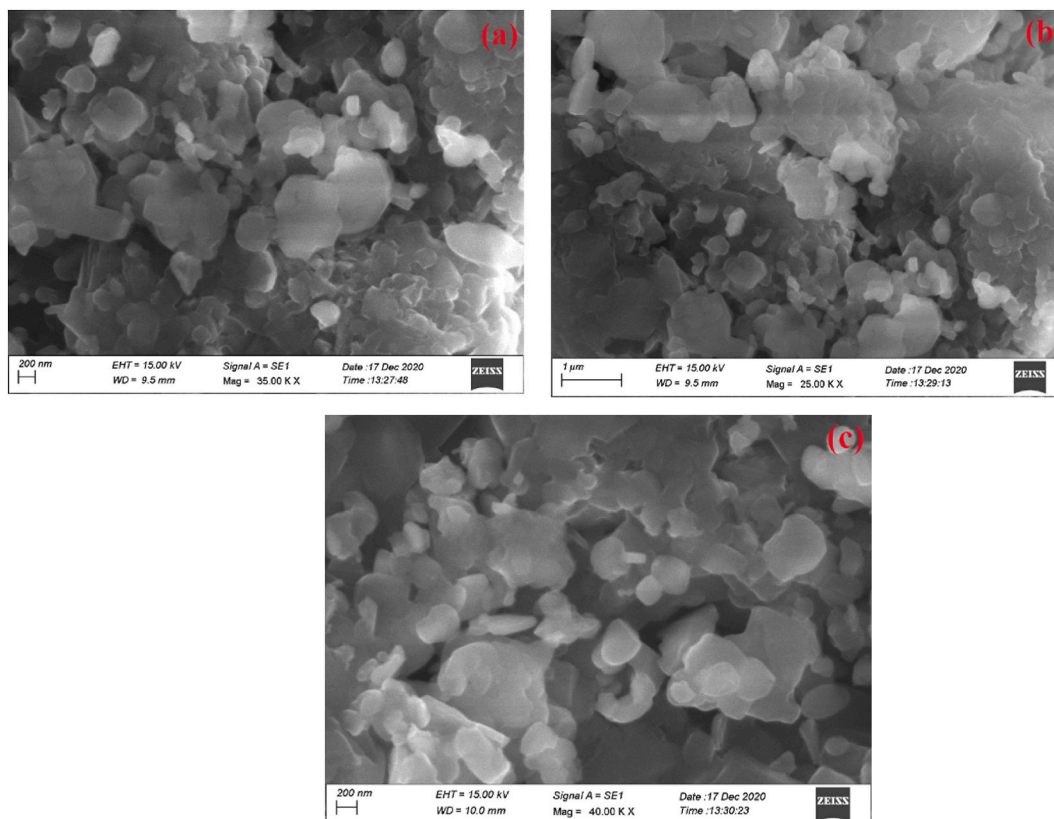


Fig. 4. (a), (b) and (c). SEM image of  $\text{MnFe}_2\text{O}_4$  at  $700^\circ\text{C}$ .

### 3.6. Energy Dispersive X-Ray Analysis (EDX)

An elemental composition of the prepared manganese ferrite nanoparticle was analyzed using Energy Dispersive X-Ray Analysis (EDX). Fig. 6 illustrates the EDX spectrum of the analyzed sample, allowing for the observation and characterization of the elements present, as well as their relative abundance [26].

The investigation of the synthesized manganese ferrite nanoparticle using Energy dispersive X-Ray analysis indicates the presence of manganese, oxygen, and iron as the primary elements, without any detected contamination from other elements [27]. The peaks observed in the EDX spectrum appropriately represent the true composition of the analyzed sample. Table 2 provides a quantitative analysis of the EDX spectrum that shows the relative proportions of the components.

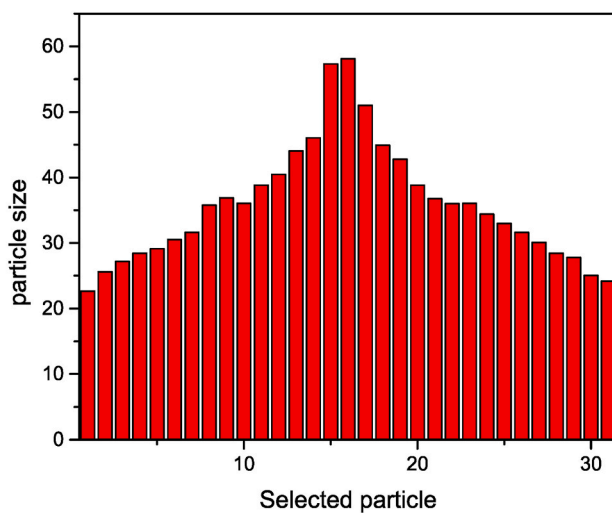
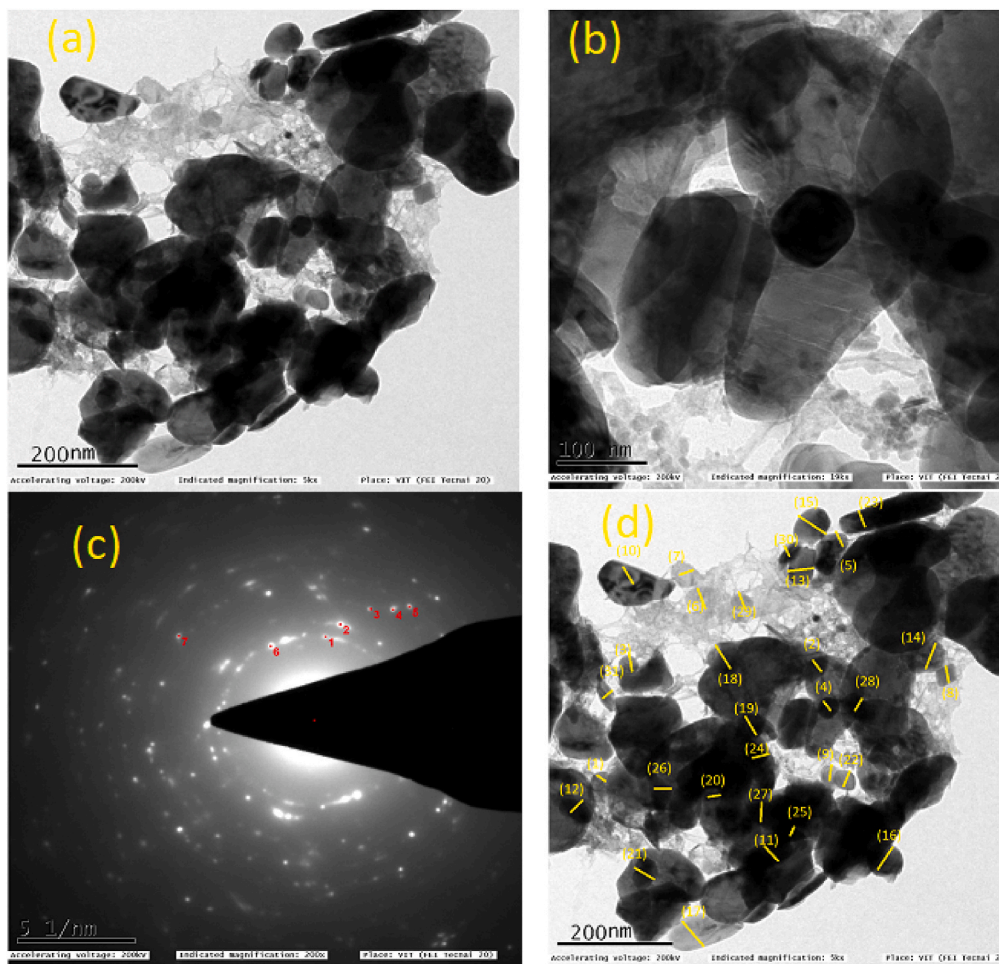
### 3.7. Brunauer - Emmett - Teller (BET)

The pore size distribution curve of  $\text{MnFe}_2\text{O}_4$  nanoparticles is shown in Fig. 7(a) illustrating the range of pore sizes present within the material. Furthermore, Fig. 7(b) showcases a typical  $\text{N}_2$  adsorption-desorption isotherm, which depicts the adsorption and desorption properties of nitrogen gas on the surface of the nanoparticles.

The inset of Fig. 7(a) indicates that the main pore size in this system is 3.0594 nm, while the mesoporous range spans from 19 to 80 nm, indicating the disorganized porosity structure. The nitrogen adsorption isotherm illustrated in Fig. 7(b) demonstrates an IV-type with a  $\text{H}_2$  hysteresis loop according to the IUPAC classification in the relative pressure ( $P/P_0$ ) that ranges from 0.0 to 1.0. The presence of mesoporous  $\text{MnFe}_2\text{O}_4$  nanoparticles is likely responsible for this observed hysteresis loop. The nitrogen adsorption analysis reveals a significant BET surface area of  $44.66 \text{ m}^2\text{g}^{-1}$  for  $\text{MnFe}_2\text{O}_4$ , exceeding previous reports on pure  $\text{MnFe}_2\text{O}_4$  nanoparticles [28,29]. The highly mesoporous nature of  $\text{MnFe}_2\text{O}_4$  provides a profusion of active sites on the surface, which plays an essential role in its super capacitive behaviour.

### 3.8. X-ray photoelectron spectroscopy (XPS)

X-ray photoelectron spectroscopy analysis is a valuable method create the quantitatively identify the surface components and composites of a sample. Fig. 8(e) illustrates the wide scan XPS spectra of the sample, covering a binding energy range of 0–900 eV. To calculate the binding energies of individual components, C1s (approximately 288 eV) (C–C), (C=O), ( $\text{CF}_2$ ) [30–32] was used as a



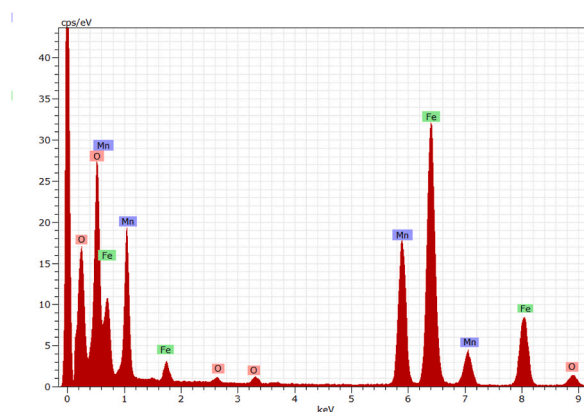
(e)

**Fig. 5.** (a), (b) HR-TEM of MnFe<sub>2</sub>O<sub>4</sub> nanoparticle annealed at 700 °C with different magnification and (c) corresponding SAED pattern, (d) particle size measured using image ‘j’ viewer software.

**Fig. 5 (e).** Average Particle size of HR-TEM by using image ‘j’ software.

**Table 1**Number of particle and particle size of  $\text{MnFe}_2\text{O}_4$  using image 'j' software from HR-TEM.

Number of particles	Particle size	Number of particles	Particle size
1	22.627	17	50.990
2	25.612	18	44.944
3	27.203	19	42.802
4	28.425	20	38.833
5	29.120	21	36.770
6	30.529	22	36.004
7	31.623	23	36.056
8	35.77	24	34.409
9	36.878	25	32.985
10	36.056	26	31.623
11	38.833	27	30.067
12	40.447	28	28.425
13	44.045	29	27.785
14	46.043	30	25.060
15	57.306	31	24.166
16	58.136	Average	35.792

**Fig. 6.** EDX analysis of the sample  $\text{MnFe}_2\text{O}_4$  at 700 °C.**Table 2**Quantitative analysis of  $\text{MnFe}_2\text{O}_4$ .

Element	Series	Net	Unn.C [wt.%]	Norm.C [wt.%]	Atom.C [at.%]	Error (3 sigma) [wt.%]
Oxygen	K-Series	24609	27.84	27.84	57.25	2.64
Iron	K-series	58235	47.65	47.65	28.07	4.41
Manganese	K-series	30911	24.51	24.51	14.68	2.33
		Total	100.00	100.00	100.00	

reference point, as shown in Fig. 8(a). Further confirmation of the individual components was achieved through specific XPS spectra of Oxygen (O1s) (OH), (Mn–O–H), (M – O) [33,34], Manganese (Mn2p<sub>3/2</sub> & Mn2p<sub>1/2</sub>) [34], and Ferrous (Fe2p<sub>1/2</sub> & Fe2p<sub>3/2</sub>) [35], demonstrates in Fig. 8 (a to d), respectively.

In Fig. 8(e), the wide scan XPS spectra of the sample reveal the observed binding energies assigned to C1s Fig. 8(a), O1s Fig. 8(b), Mn2p Fig. 8(c), and Fe2p Fig. 8(d) on the surface of the Fe<sub>2</sub> composite, including Mn–O<sub>4</sub> and MnFe<sub>2</sub>O<sub>4</sub>. The binding energies of the individual components, namely C1s, O1s, Mn2p, and Fe2p, are summarized in Table 3.

It is significant to observe that the full width at half maximum remains consistent for each spin-orbit component, except for Mn2p and Mn2p<sub>1</sub>, where the latter exhibits broader peaks. This broadening is attributed to the Coster-Kronig effect (post-ionization). The Mn2p<sub>1</sub> peak appears smaller when compared to Mn2p.

The XPS results provide evidence and confirm the existence of Mn<sup>2+</sup> and Fe<sup>2+</sup> on the surface of the MnFe<sub>2</sub>O<sub>4</sub> sample supporting previous findings [36,37].

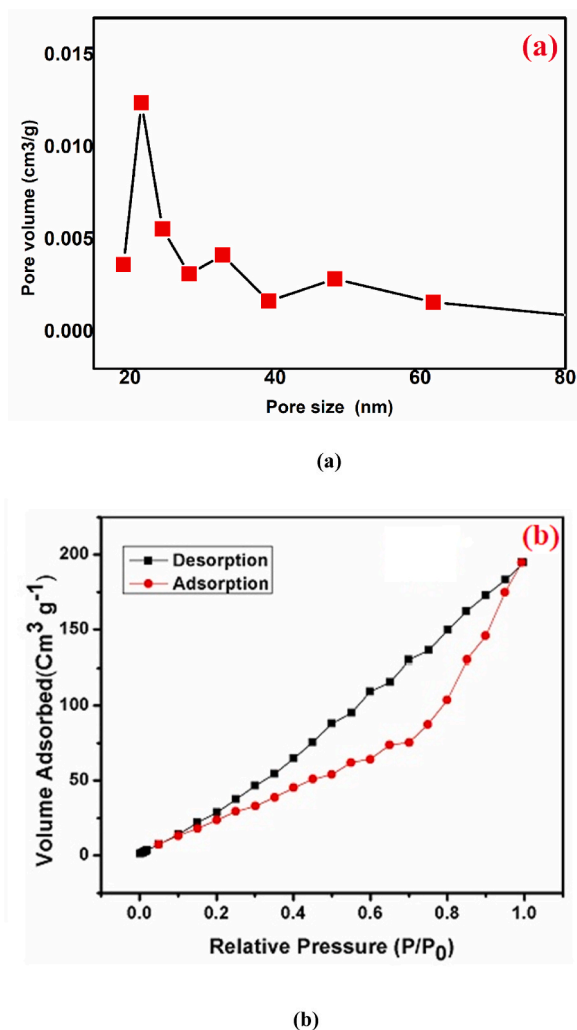


Fig. 7. (a) Pore distribution of MnFe<sub>2</sub>O<sub>4</sub>  
 Fig. 7(b) N<sub>2</sub> adsorption-desorption isotherm.

### 3.9. Cyclic voltammetry

The capacitive behaviour of a MnFe<sub>2</sub>O<sub>4</sub> electrode was examined through cyclic voltammetry (CV), an electrochemical technique. The CV measurements were performed at various scan rates of (2, 5, and 10 mVs<sup>-1</sup>) and the results were shown in Fig. 9. At lower scan rates, the CV curves display an ideal rectangular shape, indicative of well-defined capacitive behaviour [38].

The CV patterns of the MnFe<sub>2</sub>O<sub>4</sub> sample, which underwent calcination at 700 °C, reveal a pseudo-capacitive nature, as evidenced by changes in the CV curves with increasing scan rate. This indicates the presence of pseudo-capacitive processes within the system, indicating a dynamic capacitive response influenced by the scan rate. The specific capacitances (C<sub>s</sub>) value of the prepared manganese ferrite electrode was determined by using the following equation [39]:

$$C_s = \frac{Q}{(\Delta v \cdot m)} \quad (2)$$

Here C<sub>s</sub> represents specific capacitance, Q denotes anodic and cathodic charges recorded during each scanning, m indicates the mass of the electrode material (in mg), and Δv represents the fixed scan rate (mVs<sup>-1</sup>) employed for the measurements. Electrochemical measurements were conducted using a typical three-electrode configuration consisting of a sample as a working electrode, an Ag/AgCl reference electrode, and a high platinum wire as a counter electrode [40]. In which 0.2 M tetra butyl ammonium perchlorate was taken as electrolyte. At a scan rate of 2 mVs<sup>-1</sup>, the highest specific capacitance value obtained is about 341.14 Fg<sup>-1</sup>. However, as the scan rate increased, the specific capacitance of the nanostructured electrodes decreased. This can be attributed to limited ion accessibility within the electrode pores at higher scan rates, resulting in only the outermost portion of the electrode being effectively utilized for ion

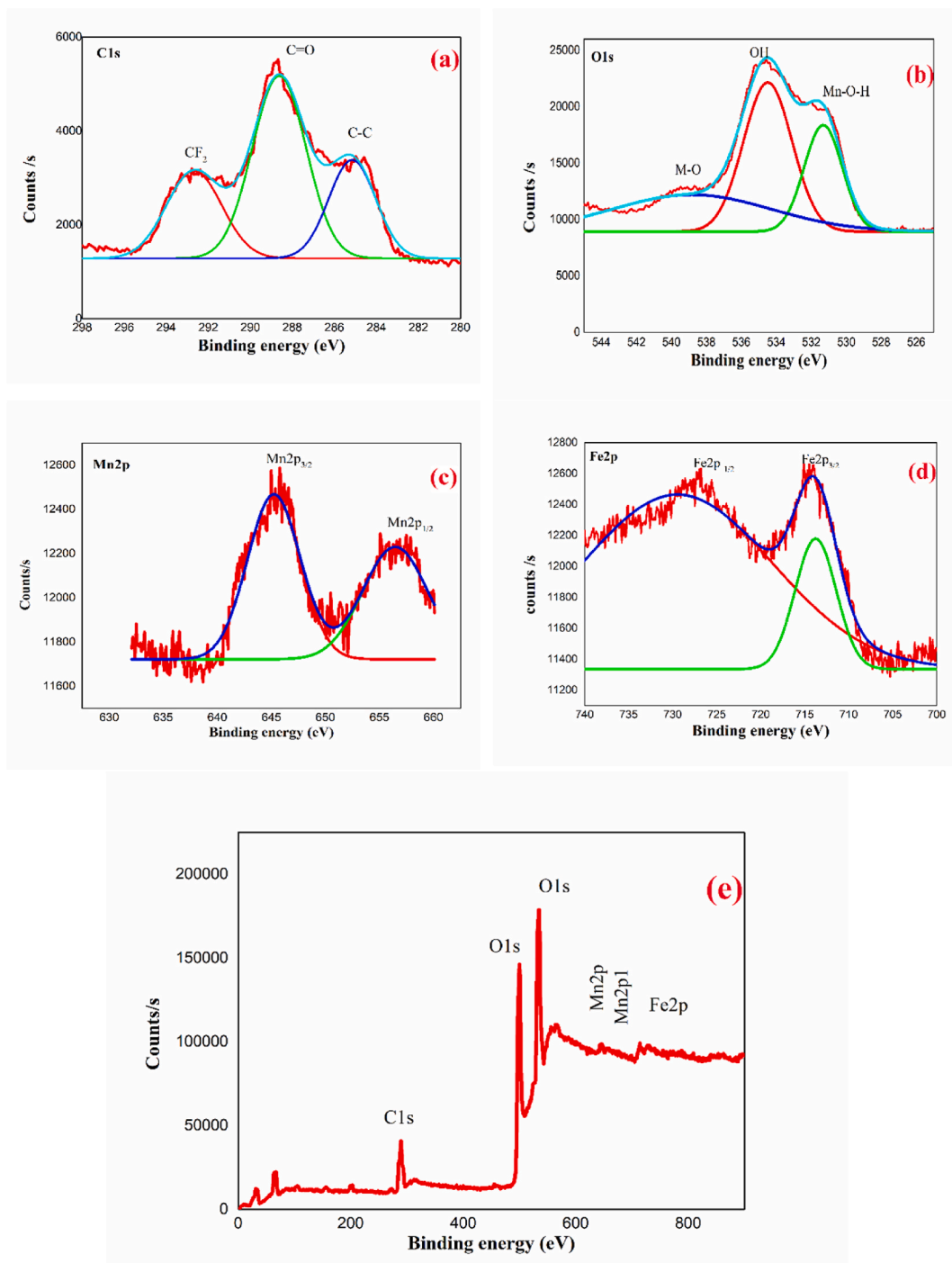


**Fig. 8.** (a), (b), (c), and (d) Deconvolute XPS spectra of C1s, O1s, Mn2p and Fe2p peak of the sample respectively and Fig. 8(e) shows wide scan XPS spectra of MnFe<sub>2</sub>O<sub>4</sub> sample.

diffusion. Specifically, at a scan rate of 10 mVs<sup>-1</sup>, the value of the specific capacitance remains at 37.524 Fg<sup>-1</sup>. The greater specific capacitance value discovered in this study indicates the good crystallinity of the manganese ferrite nanoparticle. In comparison to the work done by Deshmukh et al., who reported a specific capacitance value is 148.4 Fg<sup>-1</sup> at a scan rate of 5 mVs<sup>-1</sup>, in the present work MnFe<sub>2</sub>O<sub>4</sub> sample demonstrated a higher specific capacitance value found at 223.7 Fg<sup>-1</sup> at the similar scan rates, indicates its better suitability for super capacitor applications [41]. The variation in specific capacitance values as the scan rate was increased from 2 to 10 mVs<sup>-1</sup> is depicted in Fig. 9 and summarized in Table 4.

**Table 3**  
Binding Energies of O1s, C1s, Mn2p and Fe2p components in the synthesized sample.

Name	Peak BE	FWHM eV	Area (P) CPS.eV	Atomic %
O1s	533.76	6.44	702959.00	82.08
C1s	288.63	2.78	23944.08	6.76
O1s	534.14	5.97	85235.01	9.96
Mn2p	645.48	5.05	5962.82	0.18
Fe2p	713.92	6.44	14227.36	0.39
Mn2p1	648.08	0.58	3565.59	0.32

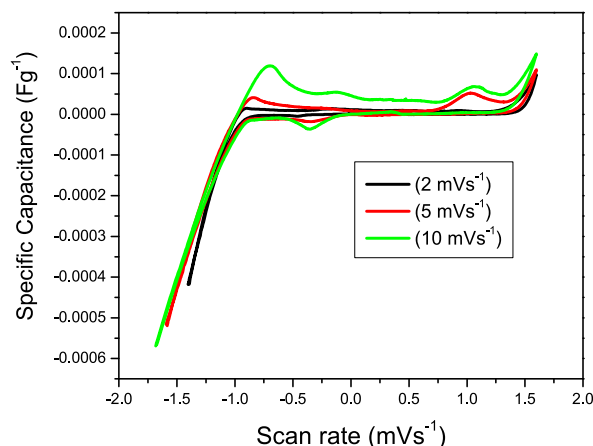


**Fig. 9.** CV pattern of manganese ferrite nanoparticle.

**Table 4**  
Specific Capacitance value of  $\text{MnFe}_2\text{O}_4$  (700 °C) at different scan rate.

Scan rate ( $\text{mVs}^{-1}$ )	Specific Capacitance ( $\text{Fg}^{-1}$ )
2	341.14
5	223.73
10	37.52

#### 4. Conclusion

The prepared sample of manganese ferrite nanoparticles was achieved through a simple co-precipitation method. Using Debye - Scherrer's formula the particle size was determined to be around 37 nm. Both SEM and HR-TEM analysis confirmed the presence of spherical-shaped particles, with HR-TEM measurements indicating a particle size of 35 nm, matching the crystallite size calculated from XRD analysis. EDX analysis demonstrated the exclusive presence of Mn, Fe, and O elements in the sample, without any detectable impurities. Electrochemical analysis was performed using cyclic voltammetry measurements to evaluate the  $\text{MnFe}_2\text{O}_4$  electrode's performance. It shows excellent specific capacitance values, reaching a maximum of  $341.14 \text{ Fg}^{-1}$  at a scan rate of  $2 \text{ mVs}^{-1}$ . This result illustrates an electrode's promising suitability for super capacitor applications and demonstrates its efficient energy storage and delivery capabilities.

#### Data availability statement

Data will be made available on request.

#### CRediT authorship contribution statement

**Abisha D:** Conceptualization, Data curation, Formal analysis, Investigation, Methodology, Resources, Software, Validation, Visualization, Writing – original draft. **Gibin S.R:** Project administration, Supervision, Writing – review & editing. **PremKumar V.K:** Resources, Validation. **Mariappan A:** Resources, Validation.

## Declaration of competing interest

Author has no conflicts of interest.

## References

- [1] S.L. Brock, Nanostructures and Nanomaterials: Synthesis, Properties and Applications by Guozhang Cao, University of Washington). Imperial College Press (distributed by World Scientific, London, 2004, 1-86094-415-9.
- [2] H. Farooq, M.R. Ahmad, Y. Jamil, A. Hafeez, Z. Mahmood, T. Mahmood, Structural and dielectric properties of manganese ferrite nanoparticles, *J. Basic Appl. Sci.* 8 (2012) 597–601.
- [3] C. Sambathkumar, M.K. Kumar, N. Nallamuthu, K. Rajesh, P. Devendran, Investigations on electrochemical performances of Co (OH) 2, Fe<sub>2</sub>O<sub>3</sub> and Mn<sub>3</sub>O<sub>4</sub> nanoparticles covered carbon micro spheres for supercapacitor application, *Inorg. Chem. Commun.* 134 (2021), 109057.
- [4] J. Amighian, M. Mozaffari, B. Nasr, Preparation of nano-sized manganese ferrite (MnFe<sub>2</sub>O<sub>4</sub>) via coprecipitation method, *Phys. Status Solidi C* 3 (9) (2006) 3188–3192.
- [5] K. Islam, M. Haque, A. Kumar, A. Hoq, F. Hyder, S.M. Hoque, Manganese ferrite nanoparticles (MnFe<sub>2</sub>O<sub>4</sub>): size dependence for hyperthermia and negative/positive contrast enhancement in MRI, *Nanomaterials* 10 (11) (2020) 2297, <https://doi.org/10.3390/nano10112297>.
- [6] U.S. Sharma, R.N. Sharma, R. Shah, Physical and magnetic properties of manganese ferrite nanoparticles, *Int. J. Eng. Res. Afr.* 4 (8) (2014) 14–17.
- [7] C. Sambathkumar, N. Nallamuthu, M.K. Kumar, S. Sudhahar, P. Devendran, Electrochemical exploration of cobalt sulfide nanoparticles synthesis using cobalt diethyldithiocarbamate as single source precursor for hybrid supercapacitor device, *J. Alloys Compd.* 920 (2022), 165839.
- [8] K. Seevakan, A. Manikandan, P. Devendran, Y. Slimani, A. Baykal, T. Alagesan, Structural, magnetic and electrochemical characterizations of Bi<sub>2</sub>MoO<sub>9</sub> nanoparticle for supercapacitor application, *J. Magn. Mater.* 486 (2019), 165254.
- [9] M. Murugesan, N. Nallamuthu, R. Ranjithkumar, M. Krishnakumar, P. Devendran, K. Ramesh, Synthesis and electrochemical investigation of hetero bimetallic complexes CoMn<sub>2</sub>O<sub>4</sub> micro rods for novel supercapacitor electrode, *Electron. Mater. Lett.* 19 (1) (2023) 108–118.
- [10] K.R. Nagavenkatesh, C. Sambathkumar, N. Nallamuthu, M.K. Kumar, P. Devendran, Investigation of electrochemical behaviour and annealing effect on zinc cobaltite nanoparticles as working electrode material for energy storage device, *J. Mater. Sci. Mater. Electron.* 33 (28) (2022) 22169–22182.
- [11] C. Sambathkumar, K.R. Nagavenkatesh, K.M. Krishna, N. Nallamuthu, S. Sudhahar, P. Devendran, Electrochemical exploration on hexadecylamine capped copper sulfide nanocubes using single source precursor for enhanced supercapacitor devices, *J. Energy Storage* 56 (2022), 105898.
- [12] S. Suganya, G. Maheshwaran, M.R. Prabhu, P. Devendran, M.K. Kumar, S. Sudhahar, Enhanced electrochemical activity of ternary Co-Mn-Zn oxide for the fabrication of hybrid supercapacitor applications, *J. Energy Storage* 56 (2022), 106057.
- [13] S.Vinothkumar, P. Hajasharif, P. Sivagurunathan, Preparation of Electrochemical and Magnetic Properties of Manganese Ferrite nanoparticles via Sol-Gel Auto Combustion Method.
- [14] P. Sivagurunathan, S.R. Gibin, Preparation and characterization of nanosized cobalt ferrite particles by co-precipitation method with citrate as chelating agent, *J. Mater. Sci. Mater. Electron.* 27 (2016) 8891–8898.
- [15] M.S. Amulya, H.P. Nagaswarupa, M.A. Kumar, C.R. Ravikumar, K.B. Kusuma, Sonochemical synthesis of MnFe<sub>2</sub>O<sub>4</sub> nanoparticles and their electrochemical and photocatalytic properties, *J. Phys. Chem. Solid.* 148 (2021), 109661, <https://doi.org/10.1016/j.jpccs.2020.109661>.
- [16] V. Vignesh, K. Subramani, M. Sathish, R. Navamathavan, Electrochemical investigation of manganese ferrites prepared via a facile synthesis route for supercapacitor applications, *Colloids Surf. A Physicochem. Eng. Asp.* 538 (2018) 668–677.
- [17] E.R. Kumar, T. Arunkumar, T. Prakash, Heat treatment effects on structural and dielectric properties of Mn substituted CuFe<sub>2</sub>O<sub>4</sub> and ZnFe<sub>2</sub>O<sub>4</sub> nanoparticles, *Superlattice. Microsc.* 85 (2015) 530–535.
- [18] P.A. Ajibade, E.C. Nnadozie, Synthesis and structural studies of manganese ferrite and zinc ferrite nanocomposites and their use as photoadsorbents for indigo carmine and methylene blue dyes, *ACS Omega* 5 (50) (2020) 32386–32394.
- [19] L.A. Kafshgari, M. Ghorbani, A. Azizi, Synthesis and characterization of manganese ferrite nanostructure by co-precipitation, sol-gel, and hydrothermal methods, *Particulate Sci. Technol.* 37 (7) (2018) 904–910.
- [20] R. Sundari, T.I. Hua, M. Aziz, D. Nizar, The characterization study of ferrites (magnesium and manganese) using sol gel method, *The Malaysian Journal of Analytical Sciences* 18 (3) (2014) 485–490.
- [21] A. Mary Jacintha, V. Umapathy, P. Neeraja, S. Rex Jeya Rajkumar, Synthesis and comparative studies of MnFe<sub>2</sub>O<sub>4</sub> nanoparticles with different natural polymers by sol-gel method: structural, morphological, optical, magnetic, catalytic and biological activities, *Journal of Nanostructure in Chemistry* 7 (2017) 375–387.
- [22] I. Elahi, R. Zahira, K. Mehmood, A. Jamil, N. Amin, Co-precipitation synthesis, physical and magnetic properties of manganese ferrite powder, *Afr. J. Pure Appl. Chem.* 6 (1) (2012) 1–5.
- [23] K. Zipare, J. Dhupal, S. Bandgar, V. Mathe, G. Shahane, Superparamagnetic manganese ferrite nanoparticles: synthesis and magnetic properties, *J. Nanosci. Nanoeng* 1 (3) (2015) 178–182.
- [24] M.M.N. Ansari, S. Khan, N. Ahmad, Effect of R<sup>3+</sup> (R = Pr, Nd, Eu and Gd) substitution on the structural, electrical, magnetic and optical properties of Mn-ferrite nanoparticles, *J. Magn. Mater.* 465 (2018) 81–87.
- [25] S. Kanagesan, S.B.Z. Aziz, M. Hashim, I. Ismail, S. Tamilselvan, N.B.B.M. Alitheen, M.K. Swamy, B. Purna Chandra Rao, Synthesis, characterization and in vitro evaluation of manganese ferrite (MnFe<sub>2</sub>O<sub>4</sub>) nanoparticles for their biocompatibility with murine breast cancer cells (4T1), *Molecules* 21 (3) (2016) 312.
- [26] M. Jacintha, P. Neeraja, M. Sivakumar, K. Chinnaraj, Comparative Study of MnFe<sub>2</sub>O<sub>4</sub> Nanoparticles synthesized by sol-gel method with two different surfactants, *J. Supercond. Nov. Magnetism* 30 (2017) 237–242.
- [27] L.X. Yang, F. Wang, Y.F. Meng, Q.H. Tang, Z.Q. Liu, Fabrication and characterization of manganese ferrite nanospheres as a magnetic adsorbent of chromium, *J. Nanomater.* 2013 (2013), 2–2.
- [28] A. Monunith, A. Rajan, N.K. Sahu, Comparative study of enzymatic and non-enzymatic detection of glucose using manganese ferrite nanoparticles, 2020, *Mater. Res. Express* 7 (9) (2020).
- [29] C.O. Ania, A. Gomis-Berenguer, J. Dentzer, C. Vix-Guterl, Nanoconfinement of glucose oxidase on mesoporous carbon electrodes with tunable pore sizes, *J. Electroanal. Chem.* 808 (2018) 372–379.
- [30] S. Oswald, F. Thoss, M. Zier, M. Hoffmann, T. Jaumann, M. Herklotz, K. Nikolowski, F. Scheiba, M. Kohl, L. Giebeler, D. Mikhailova, Binding energy referencing for XPS in alkali metal-based battery materials research (II): application to complex composite electrodes, *Batteries* 4 (3) (2018) 36.
- [31] A. Fujimoto, Y. Yamada, M. Koinuma, S. Sato, Origins of sp<sup>3</sup>C peaks in C1s X-ray photoelectron spectra of carbon materials, *Anal. Chem.* 88 (12) (2016) 6110–6114.
- [32] A. Dolgov, D. Lopaev, C.J. Lee, E. Zoethout, V. Medvedev, O. Yakushev, F. Bijkerk, Characterization of carbon contamination under ion and hot atom bombardment in a tin-plasma extreme ultraviolet light source, *Appl. Surf. Sci.* 353 (2015) 708–713.
- [33] H.M. Luo, Y.X. Sun, F.B. Zhang, D.Y. Zhang, Y.F.Y.J.Q. Zhang, Preparation and electrochemical applications of spherical maltose-based templated carbon/MnOx composite materials, *Electrochim. Acta* 148 (2014) 228–236.
- [34] S.E. Arasi, R. Ranjithkumar, P. Devendran, M. Krishnakumar, A. Arivarasan, Investigation on electrochemical behaviour of manganese vanadate nanopebbles as potential electrode material for supercapacitors, *J. Alloys Compd.* 857 (2021), 157628.
- [35] M.H. Hamed, R.A. Hinz, P. Lomker, M. Wilhelm, Gloskovskii, P. Bencok, C. Schmitz-Antoniak, H. Elnaggar, C.M. Schneider, M. Muller, Tunable magnetic phases at Fe<sub>3</sub>O<sub>4</sub>/SrTiO<sub>3</sub> oxide interfaces, *ACS Appl. Mater. Interfaces* 11 (7) (2019) 7576–7583.
- [36] Y. Yan, X. Zhang, Y. Huang, Q. Ding, X. Pang, Antibacterial and bioactivity of silver substituted hydroxyapatite/TiO<sub>2</sub> nanotube composite coatings on titanium, *Appl. Surf. Sci.* 314 (2014) 348–357.

- [37] J.M. Jang, S.W. Chung, H.C. Choe, W.A. Brantley, Electrochemical deposition behavior and characterization of Pd-Ag-HAp nanoparticles on ultra-fine TiO<sub>2</sub> nanotubes, *Surf. Coating. Technol.* 320 (2017) 383–390.
- [38] S.R. Gibin, P. Sivagurunathan, Synthesis and characterization of nickel cobalt ferrite (Ni<sub>1-x</sub>Co<sub>x</sub>Fe<sub>2</sub>O<sub>4</sub>) nano particles by co-precipitation method with citrate as chelating agent, *J. Mater. Sci. Mater. Electron.* 28 (2017) 1985–1996.
- [39] K. Sathishkumar, N. Shanmugam, N. Kannadasan, S. Cholan, G. Viruthagiri, Opto, magnetic and electrochemical characterization of Ni<sub>1-x</sub>Co<sub>x</sub>O nanocrystals, *J. Mater. Sci. Mater. Electron.* 26 (2015) 1881–1889.
- [40] S.C. Pang, B.H. Wee, S.F. Chin, The capacitive behaviors of manganese dioxide thin-film electrochemical capacitor prototypes, *Int. J. Electrochem.* 2011 (2011).
- [41] V.V. Deshmukh, P.A. Nagpure, D.K. Burghate, Nanoparticles, *International Journal of Current Research* 8 (8) (2016) 35988–35991.